Electronic Supplementary Material (ESI) for Journal of Materials Chemistry A.

Self-Cleaning Intraoral Flex-Occlusometer Based on Superhydrophobic Capacitive Sensors for Dental Health Monitoring

Xin Sun, [‡ a] *Ziyi Dai,* [‡ * a] *Zijie Zhang,* [‡ b] *Xiaoli Fan,* [a] *He Zhu,* [a] *Zhiwei Fu,* [a] *Rong Cai,* [* c] *and Kai Qian* [* a]

[a] School of Integrated Circuits, Shandong University, Jinan, 250100, China.

[b] Department of Orthodontics, School and Hospital of Stomatology, Cheeloo College of Medicine, Shandong University & Shandong Key Laboratory of Oral Tissue Regeneration & Shandong Engineering Laboratory for Dental Materials and Oral Tissue Regeneration & Shandong Provincial Clinical Research Center for Oral Diseases, Jinan, 250012, China

[c] School of Pharmaceutical Sciences, Shandong University, Jinan, 250012, China

*E-mail: ziyidai@sdu.edu.cn, rongcai@sdu.edu.cn, kaiqian@sdu.edu.cn

‡ These authors contributed equally to this work.

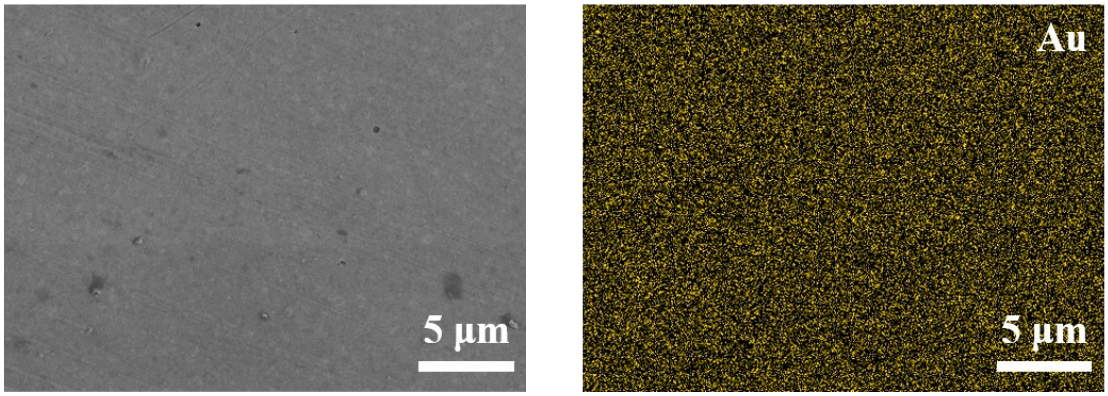

Fig. S1. Scanning electron microscope (SEM) image and EDS elemental mapping of gold electrode.

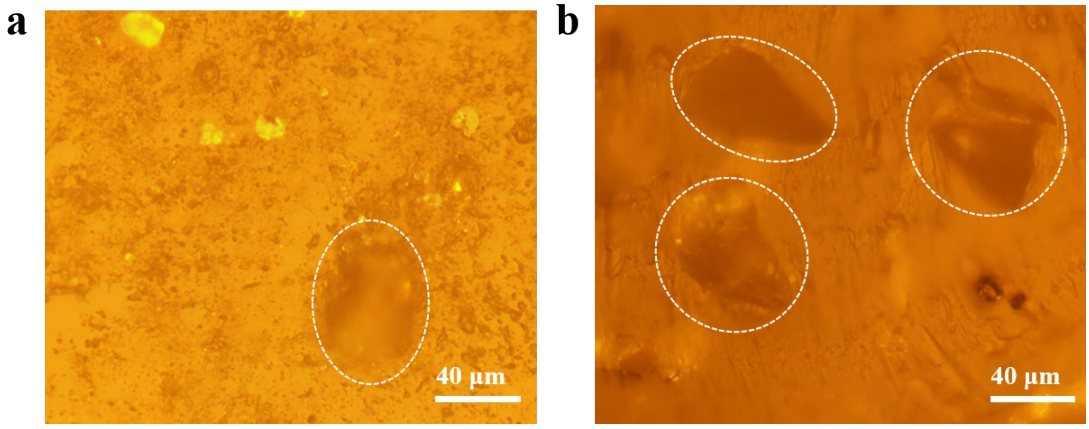

Fig. S2. (a) Plane optical microscope photo of the 3D porous structure. (b) Cross-sectional optical microscope photo of the 3D porous structure. (The white dashed circles in the images mark the location of the holes)

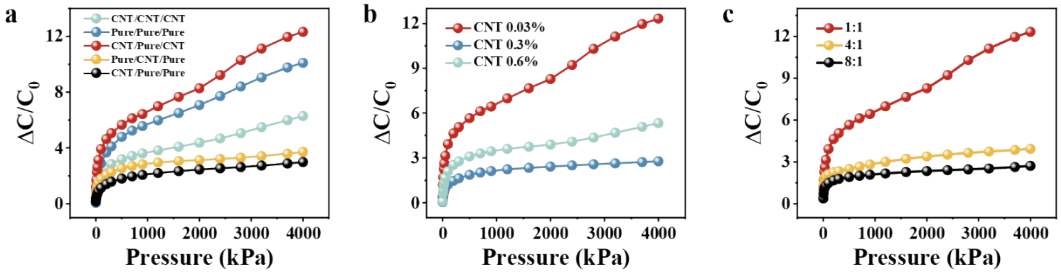

Fig. S3. (a) Sensitivity comparison of the full arrangement of three dielectric layers in sandwich structure. Contrast of sensitivity of sensors with (b)different CNT and (c) sugar content (PDMS : sugar = 1:1, 4:1, 8:1)

In order to optimize the sensing range and sensitivity of the sensor, the compression-response behavior of the sensor based on porous pure PDMS was compared with those based on porous PDMS/CNT and porous PDMS/CNT sandwich structures. **Fig. S2a** shows the results of these comparisons under the same applied pressure conditions. Sensors based on pure PDMS are easy to compress due to their low elastic modulus, and the structure reaches a solid state after all pores are completely closed. This results in a significant reduction in the sensitivity of the sensor. However, the porous PDMS/CNT is still porous, that is, the pores are open. This is because the addition of carbon nanotubes enhances the mechanical properties of the structure. Maintain a porous state in a wide pressure range. However, when the CNT concentration was increased, the sensitivity was rather reduced. This characteristic was caused by the rise of the elastic resistance of the porous structure, and the mechanical properties that were excessively reinforced by CNTs had a more negative effect on the sensor sensitivity. As a result, sensors based on porous PDMS/CNT sandwich structure have higher linearity than others. [1] In the case of the sensor with 0.03 wt % CNTs **(Fig. S2b)**, the pores are still in the opened state and the sensor has high linearity due

to linear deformation under high pressures. Additionally, the percolation effect is boosted by the CNTs, resulting in a higher sensitivity than that of the sensor based on pristine PDMS. With the principle of a, when the CNT content is too high, the sensitivity of the sensor will be reduced. [1] Besides, **Fig. S2c** shows that PDMS exhibit the highest sensitivity when the sugar to mass ratio is 1:1, because porous PDMS prepared with a high sugar to mass ratio have a high pore area ratio in both horizontal and vertical cross sections. [2]

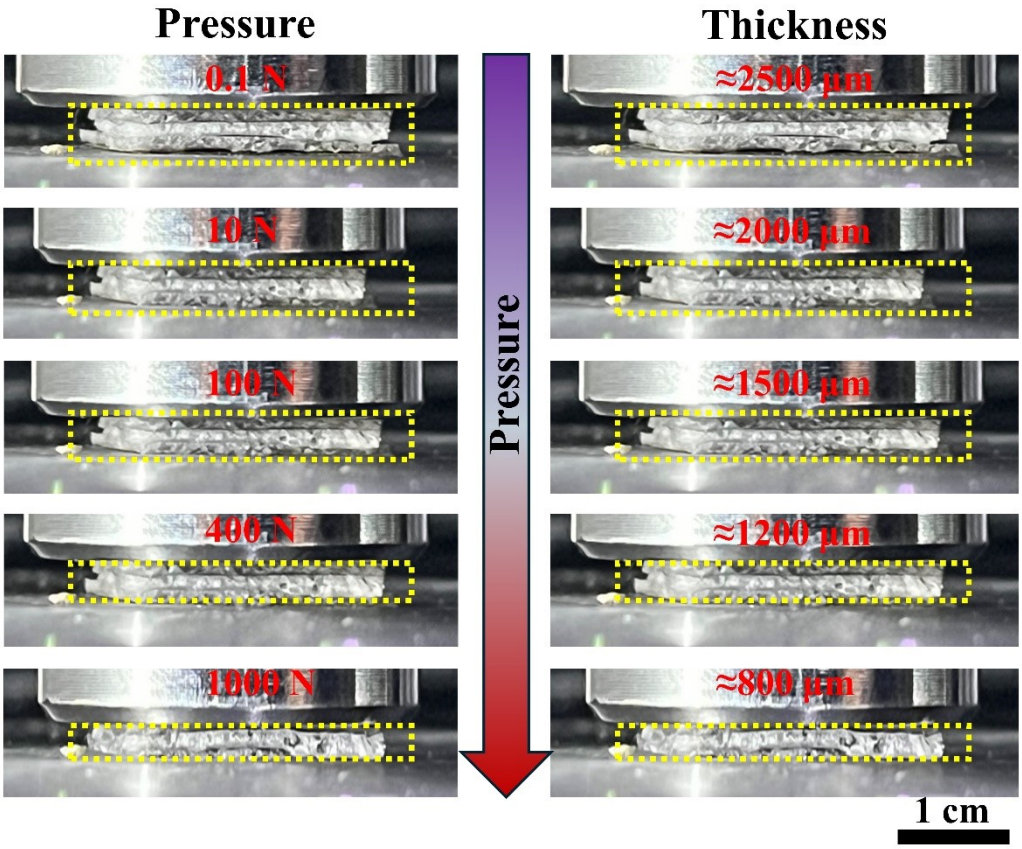

Fig. S4. Optical images of the flex-occlusometer under various pressure tests are provided alongside corresponding variations in thickness

Fig. S5. Photograph of testing platform for evaluating the sensing performance of the flex-occlusometer, comprising a mechanical triggering platform and an electrical signal monitoring system.

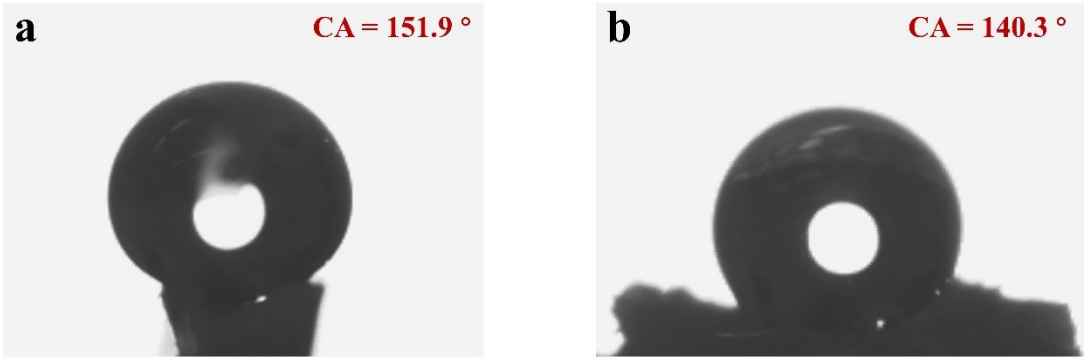

Fig. S6. (a) Optical image of the resident droplet on the vertical cross-section of the superhydrophobic pressure sensor. (b) Optical image showcasing the resident droplet on the horizontal cross-section of the superhydrophobic pressure sensor.

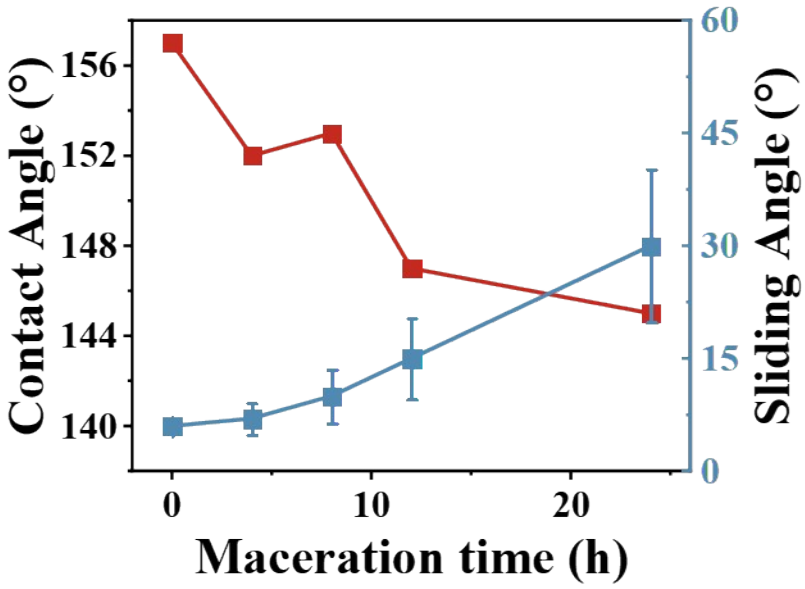

Fig. S7. Variation in θ_{CA} and θ_{SA} in the NaOH solution (PH=12).

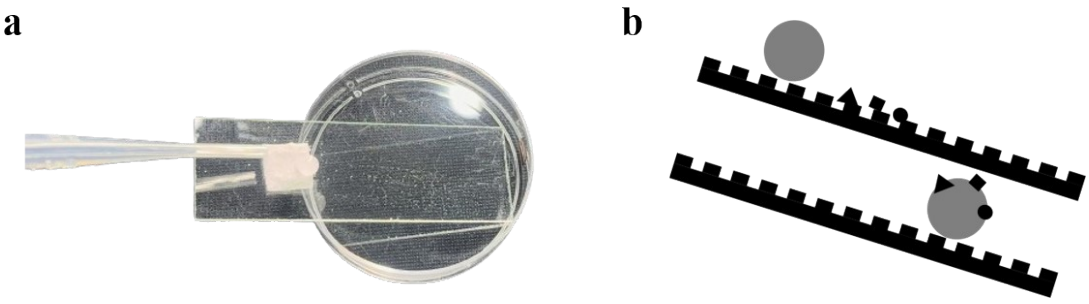

Fig. S8. (a) Optical image of the self-cleaning performance of the flex-occlusometer to remove NaCl. (b) Self-cleaning schematic diagram due to superhydrophobic surface.

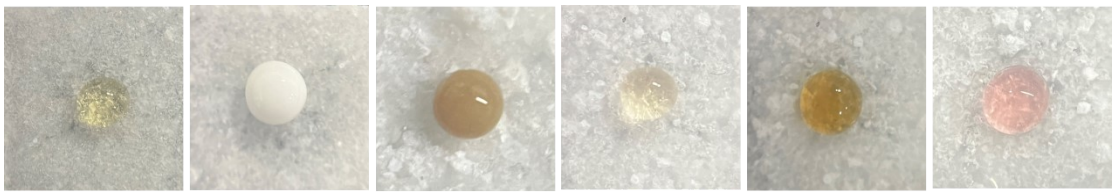

Fig. S9. Optical images of various beverages droplets on flex-occlusometer with spherical cap-shape in non-wetting state including tea, milk, milk tea, plum syrup, coffee and grape juice.

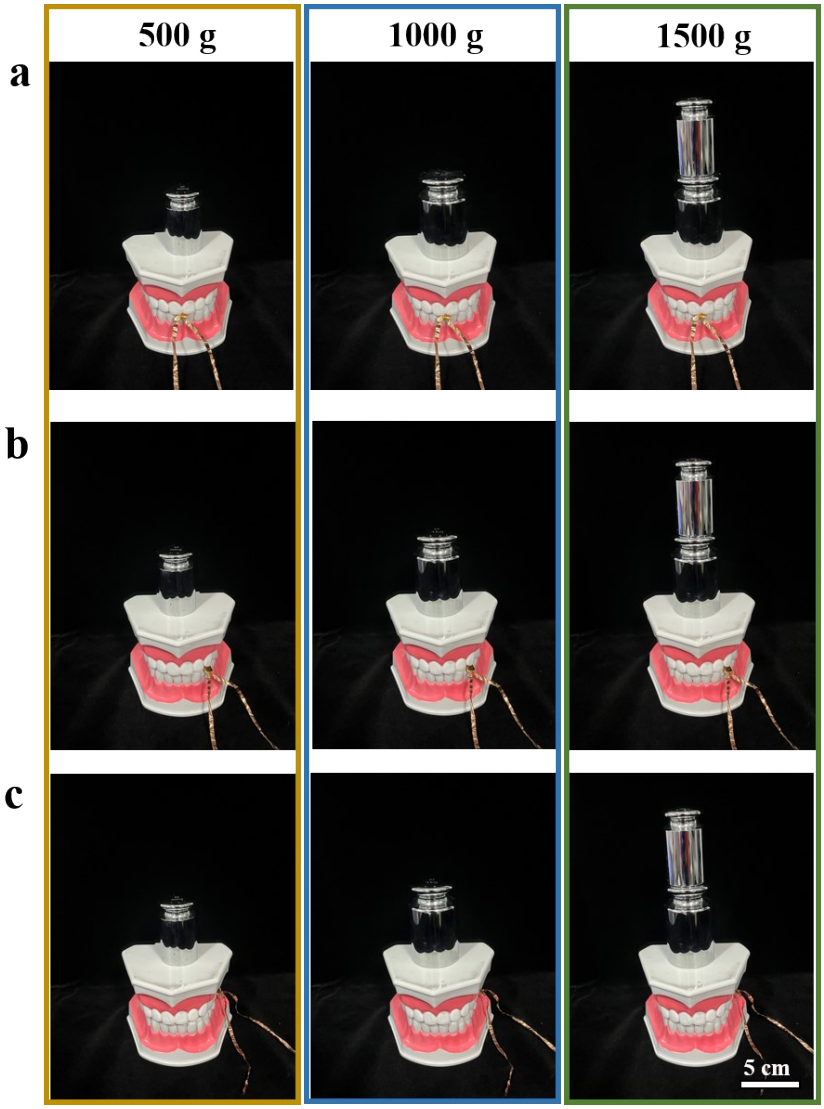

Fig. S10. Photographs of the sensing performance testing plateform of the flex-occlusometer on model teeth. Specific bite forces were applied using weights, with test locations including (a) incisors, (b) canines, and (c) molars.

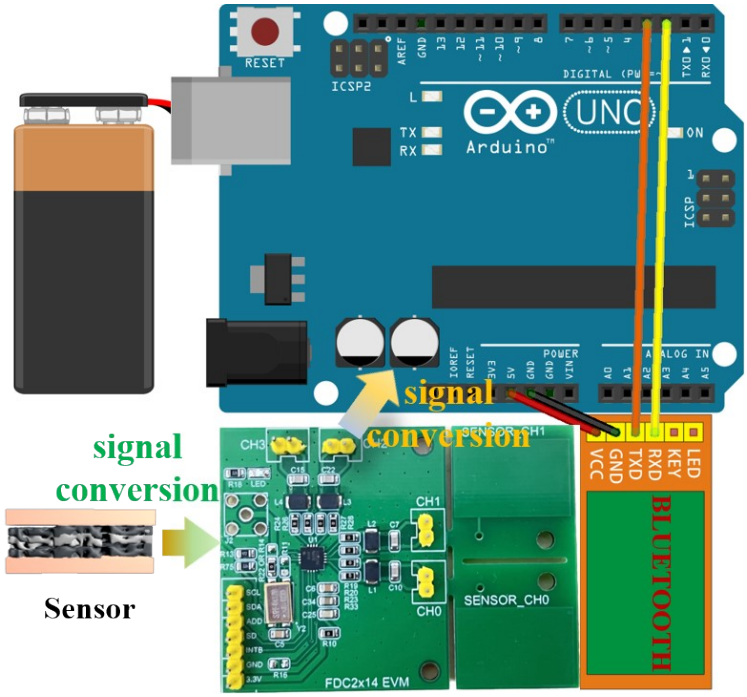

Fig. S11. Circuit diagram of wireless monitoring occlusal instrument.

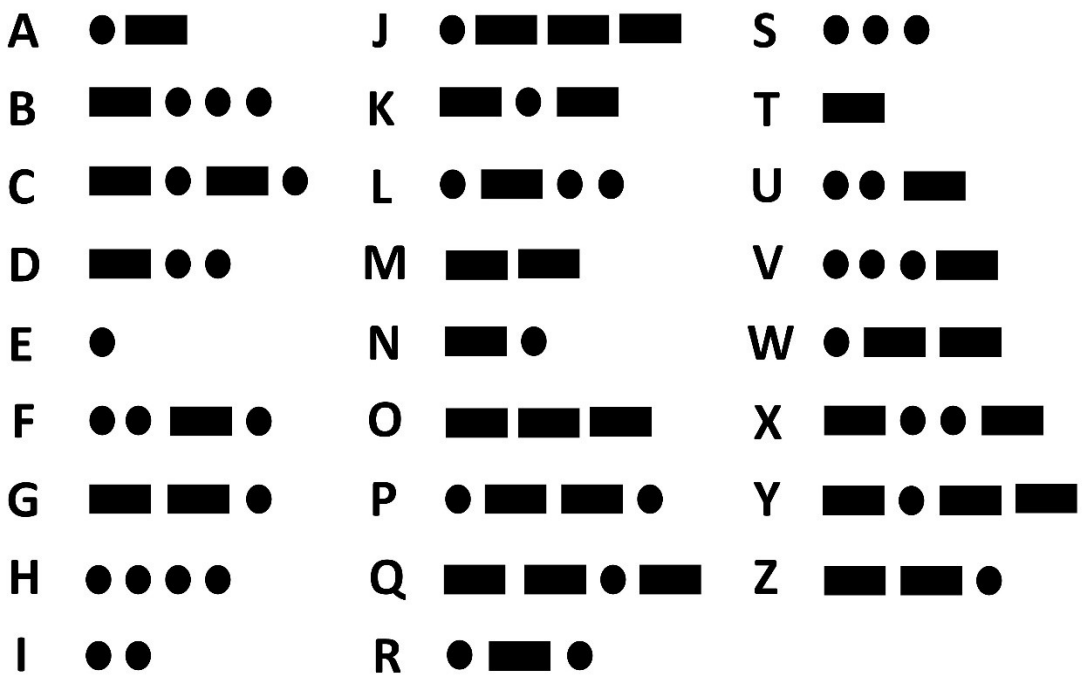

Fig. S12. Morse Code Comparison Table for the 26 Letters of the Alphabet. (We differentiate between dot and dash by controlling the duration of the capacitor signal.)

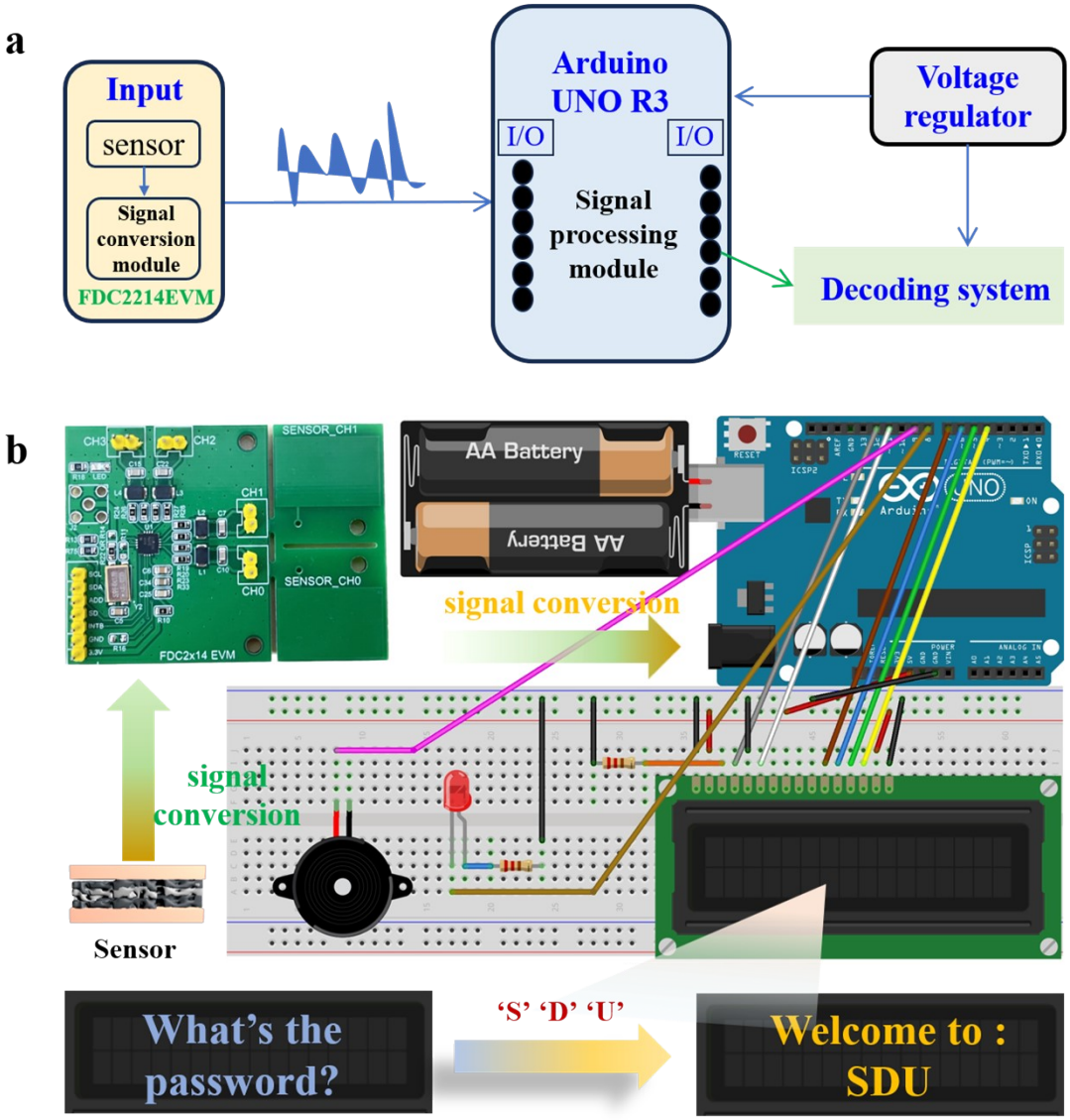

Fig. S13. Circuit diagram of Morse code decoding system.

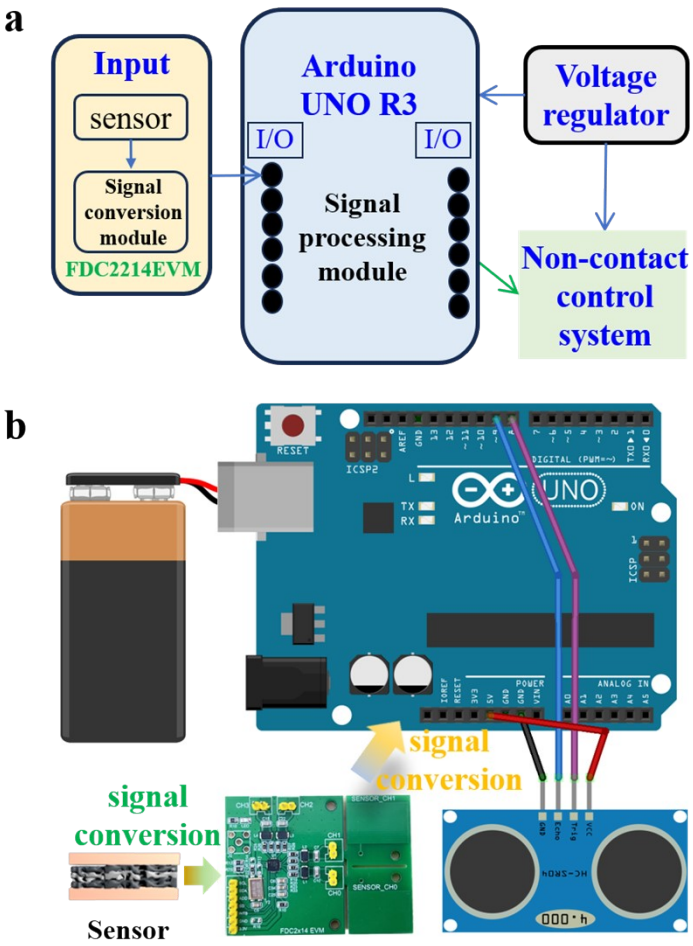

Fig. S14. Circuit diagram of contactless control play system.

Table S1. Comparison of the flex-occlusometer with the pressure sensors reported in the literature

Sensor Materials	Pressure range (kPa)	Super-hydrophobicity	Ref.
Porous PDMS	**1000**	**No**	**3**
PDMS/AgNP	**200**	**No**	**4**
PDMS/CNT	**1000**	**No**	**5**
Ecoflex/CNT	**50**	**No**	**6**
Laser-scribed graphene	**50**	**No**	**7**
Sponge Graphene Aerogel	**1000**	**No**	**8**
MXene/Fiber/PDMS	**2500**	**No**	**9**
PDMS/GNP	**500**	**No**	**10**
PI/CNT	**3000**	**No**	**11**
Flex-occlusometer	**4000**	**Yes**	**This work**

Table S2. Volunteers bite force measured information

Volunteers	Gender	Age	Occlusal interval
Volunteer 1	female	25	145-150 N
Volunteer 2	male	23	155-160 N
Volunteer 3	male	25	165-170 N
Volunteer 4	female	26	140-145 N
Volunteer 5	female	25	195-200 N
Volunteer 6	male	27	180-185 N
Volunteer 7	male	26	235-240 N
Volunteer 8	male	26	285-290 N
Volunteer 9	male	28	260-265 N
Volunteer 10	male	27	245-250 N

To assess the practical application of the flex-occlusometer, we conducted occlusal force testing with ten volunteers. Each participant, without being informed of the experimental purpose, placed the device on their front teeth and performed ten repetitive bites. The wireless system recorded the ten data points for each volunteer, and we calculated the mean values and ranges of fluctuation (in table). The results demonstrate that, based on occlusal habits and anatomical evidence, there are inherent differences in occlusal force between individuals. By using 5 N intervals, we can effectively distinguish and identify people based on their occlusal force, achieving an accuracy rate of 84%. This finding highlights the potential of the flex-occlusometer for personalized, privacy-oriented applications.

Movie S1. The self-cleaning capabilities of the superhydrophobic device compared to untreated surfaces.

Movie S2. Wireless flex-occlusometer system.

Movie S3. A simple Morse code decoding system.

Movie S4. The video pause control system.

Supplementary Text

Comparison of the signal-to-noise ratio (SNR) alterations, preceding and following superhydrophobic modification application to the Flex-Occlusometer, has evidenced the meaning of modification. This juxtaposition underscores the marked enhancement in device performance imparted by said modification. Under aqueous conditions, thorough examination of the Flex-Occlusometer's functionality was conducted employing the standard SNR calculation:

$$SNR = \frac{S}{N} \tag{1}$$

According to the data presented in Figure 3i, the SNR of the unmodified sensor experienced a considerable reduction of 14% under aqueous conditions, thereby inducing signal distortion. In contrast, the superhydrophobic variant of the self-cleaning Flex-Occlusometer, as depicted in Figure 3j, demonstrated a SNR of 1153%, emphasizing a significant improvement in signal detection accuracy amidst the representative ambient noise of the intricate oral cavity setting.

$$SNR = 20\log_{10}\frac{S}{N} \tag{2}$$

According to the traditional SNR logarithmic calculation formula (2), the SNR of unmodified Flex-Occlusometers is -17 dB, while the SNR of the superhydrophobic version of the Flex-Occlusometer is 21 dB.

REFERENCES

[1] Y. Jung, T. Lee, J. Oh, B.-G. Park, J.S. Ko, H. Kim, J.P. Yun, H. Cho, Linearly Sensitive Pressure Sensor Based on a Porous Multistacked Composite Structure with Controlled Mechanical and Electrical Properties, ACS Applied Materials & Interfaces 13(24) (2021) 28975-28984. https://doi.org/10.1021/acsami.1c07640.

[2] X. Su, H. Yu, C. Sun, Z. Sun, X. Li, D. Li, Microzone Melting Method of Porous Reactor Fabrication with Structure-Controlled Microchannel Networks for High Yield In Situ DNA Synthesis, ACS Applied Polymer Materials 6(1) (2024) 350-361. https://doi.org/10.1021/acsapm.3c02052.

[3] S. Chen, B. Zhuo, X. Guo, Large Area One-Step Facile Processing of Microstructured Elastomeric Dielectric Film for High Sensitivity and Durable Sensing over Wide Pressure Range, ACS Applied Materials & Interfaces 8(31) (2016) 20364-20370. https://doi.org/10.1021/acsami.6b05177.

[4] S. Zhao, R. Zhu, High Sensitivity and Broad Range Flexible Pressure Sensor Using Multilayered Porous PDMS/AgNP Sponge, Advanced Materials Technologies 4(9) (2019) 1900414. https://doi.org/10.1002/admt.201900414.

[5] X. Fu, J. Zhang, J. Xiao, Y. Kang, L. Yu, C. Jiang, Y. Pan, H. Dong, S. Gao, Y. Wang, A high-resolution, ultrabroad-range and sensitive capacitive tactile sensor based on a CNT/PDMS composite for robotic hands, Nanoscale 13(44) (2021) 18780-18788. https://doi.org/10.1039/D1NR03265H.

[6] K.H. Ha, W. Zhang, H. Jang, S. Kang, L. Wang, P. Tan, H. Hwang, N. Lu, Highly Sensitive Capacitive Pressure Sensors over a Wide Pressure Range Enabled by the Hybrid Responses of a Highly Porous Nanocomposite, Advanced Materials 33(48)

(2021) 2103320. https://doi.org/10.1002/adma.202103320.

[7] H. Tian, Y. Shu, X.-F. Wang, M.A. Mohammad, Z. Bie, Q.-Y. Xie, C. Li, W.-T. Mi, Y. Yang, T.-L. Ren, A Graphene-Based Resistive Pressure Sensor with Record-High Sensitivity in a Wide Pressure Range, Scientific Reports 5(1) (2015) 8603. https://doi.org/10.1038/srep08603.

[8] Z. Yue, Y. Zhu, J. Xia, Y. Wang, X. Ye, H. Jiang, H. Jia, Y. Lin, C. Jia, Sponge Graphene Aerogel Pressure Sensors with an Extremely Wide Operation Range for Human Recognition and Motion Detection, ACS Applied Electronic Materials 3(3) (2021) 1301-1310. https://doi.org/10.1021/acsaelm.0c01095.

[9] W.-B. Zhu, H.-S. Luo, Z.-H. Tang, H. Zhang, T. Fan, Y.-Y. Wang, P. Huang, Y.-Q. Li, S.-Y. Fu, $Ti_3C_2T_x$ MXene/Bamboo Fiber/PDMS Pressure Sensor with Simultaneous Ultrawide Linear Sensing Range, Superb Environmental Stability, and Excellent Biocompatibility, ACS Sustainable Chemistry & Engineering 10(11) (2022) 3546-3556. https://doi.org/10.1021/acssuschemeng.1c07994.

[10] H. Kou, L. Zhang, Q. Tan, G. Liu, H. Dong, W. Zhang, J. Xiong, Wireless wide-range pressure sensor based on graphene/PDMS sponge for tactile monitoring, Scientific Reports 9(1) (2019) 3916. https://doi.org/10.1038/s41598-019-40828-8.

[11] Y. Jeong, J. Gu, J. Byun, J. Ahn, J. Byun, K. Kim, J. Park, J. Ko, J.-h. Jeong, M. Amjadi, I. Park, Ultra-Wide Range Pressure Sensor Based on a Mic rostructured Conductive Nanocomposite for Wearable Workout Monitoring, Adv anced Healthcare Materials 10(9) (2021) 2001461. https://doi.org/https://doi.org/10.1002/adhm.202001461.